Available online at www.sciencedirect.com

ScienceDirect

Energy Procedia 49 (2014) 1379 – 1390

Energy Procedia

SolarPACES 2013

On the CFD&HT of the flow around a parabolic trough solar collector under real working conditions

A.A. Hachicha[1], I. Rodríguez[1], O. Lehmkuhl[2] and A. Oliva[1]*

[1] *Heat and Mass Transfer Technological Center (CTTC). Universitat Politècnica de Catalunya BarcelonaTech (UPC). ETSEIAT Colom 11, 08222, Terrassa, Spain.*

[2]*Termo Fluids, S.L. Avda. Jaquard, 97, 1-E, 08222 Terrassa. Spain. E-mail: termofluids@termofluids.com*

Abstract

Parabolic trough solar collector is currently one of the most mature and prominent solar applications for production of electricity. These systems are usually located in open terrain where strong winds may occur and affect their stability and optical performance, as well as, the heat exchange between the solar receiver and the ambient air. In this context, a wind flow analysis around a parabolic trough solar collector under real working conditions is performed. A numerical aerodynamic and heat transfer study based on Large Eddy Simulations is carried out to characterize the wind loads and the heat transfer coefficients. Computations are performed for two Reynolds number $Re_{W1}=3.9\times10^5$ and $Re_{W2}=1\times10^6$ and various pitch angles. The effects of wind speed and pitch angle on the averaged and instantaneous flow have been assessed. The aerodynamic coefficients are calculated around the solar collector and validated with measurements performed in wind tunnel tests. The variation of the heat transfer coefficient around the heat collector element with the Reynolds number is presented and compared to the circular cylinder in cross flow.

Selection and peer review by the scientific conference committee of SolarPACES 2013 under responsibility of PSE AG.

Final manuscript published as received without editorial corrections.

Keywords: Parabolic trough solar collector; wind speed effects; large-eddy simulations; heat transfer coefficient

* Corresponding author. Tel.: +34 93 739 8192; fax: +34 93 739 8101.
E-mail address: cttc@cttc.upc.edu

Selection and peer review by the scientific conference committee of SolarPACES 2013 under responsibility of PSE AG.
Final manuscript published as received without editorial corrections.
doi:10.1016/j.egypro.2014.03.147

1. Introduction

Parabolic trough solar collectors (PTC) are considered as one of the most mature, successful, and proven solar technologies for electricity generation. PTCs are typically operated at 400º C and synthetic oil is commonly used as heat transfer fluid (HTF). A PTC consists of a parabolic trough-shaped mirror that focus sun rays onto a heat collector element (HCE) that is mounted in the focal line of the parabola. The HTF circulates through the solar field to transport the absorbed heat. The solar field is made up of several solar reflectors composed in series which concentrate the direct solar radiation by means of a Sun-tracking system. The HCE is typically composed of a metal receiver tube and a glass envelope covering it with a vacuum between these two to reduce the convective heat losses.

The thermal and optical performances of PTC are related to the wind load on the structure and the tracking system. During real working conditions, the array field of solar collectors requires a good accuracy in terms of both mechanical strength and optical precision. Such requirements are sensitive to turbulent wind conditions and should be considered in the design of these systems. Hence, a wind flow analysis plays a major role for designing the solar collectors and can lead to better understanding of the aerodynamic loading around the parabolic reflector, as well as, the convection heat transfer from the HCE.

Several numerical and experimental studies have been performed to determine the thermal performance and heat transfer characteristics of PTC [1,2,3,4]. However, only few studies of wind flow around the PTC have been published. Hosoya and Peterka [5] conducted a series of wind tunnel tests about a PTC with different configurations in which they included the peak load and the local pressure across the face of the solar collector and, investigated the effect of the location of the PTC in the collector field, as well as, the use of a porous fence. Gong et al. [6] performed field measurements on the Yan Qing solar collector in China to determine the boundary layer wind characteristics and the effect of wind loads on solar collectors for different configurations.

The majority of the numerical studies for studying wind flow around solar collectors are based on the time-averaged Navier Stokes equations (RANS) [7,8] which suffer from inaccuracies in predictions of flow with massive separations [9]. Recently, Hachicha et al. [10] proposed a Large Eddy Simulations model to quantify the fluid flow and heat transfer around a PTC for various pitch angles and a fixed wind speed 1 m/s. The aim of this work is to study the impact of wind speed on the fluid flow and heat transfer around a PTC under real working conditions. To do this, the wind flow around the PTC at a wind speed of 3 m/s is studied and compared to the results obtained at 1 m/s.

2. Numerical model

The same methodology presented in the previous work [10] for solving the fluid flow and heat transfer around the PTC is adopted. This methodology has been proven and validated in turbulent flows around bluff bodies with massive separations and recirculation [11,12,13].

Simulations are performed using the CFD &HT code Termofluids [14] which is an unstructured and parallel object-oriented code for solving industrial flows.

3. Results

The suitability of the present numerical model for solving the flow around a PTC at different wind speeds and pitch angles is presented hereafter. First, a comparative for a circular cylinder in cross-flow is carried out and the wind speed effect on the heat characteristics around the circular cylinder is studied. Then, a wind flow study and wind speed effects around a PTC is performed. The results of both cases are compared against available experimental measurements from literature.

3.1. Heat transfer from a circular cylinder in cross flow and wind speed effects

The numerical model has been previously [10] applied in a circular cylinder on cross flow for Re_D=7200. Pressure distribution and heat transfer characteristics around circular cylinder have been validated respect to experimental measurements. In this work, simulations are performed for higher Reynolds number Re_D=21600 (based on the cylinder diameter and the free-stream velocity) and heat transfer characteristics are compared for both Reynolds numbers. The computational domain is extended to [-15D,25D] [-10D,10D] [0, πD] in the stream-, cross- and span-wise directions respectively, and the cylinder with a diameter D is placed at (0,0,0). The results shown herein are computed for a grid of 130000×64 planes (i.e. 130000 CVs in the 2D plane extruded in 64 planes yielding about 8.3MCVs).

For both Reynolds numbers simulated Prandtl number (Pr=ν/α) is set to Pr=0.7. Cylinder wall temperature is set to 350K and free stream temperature is maintained at 300K. The boundary conditions at the inflow consist of uniform velocity and temperature. Slip and Neumann conditions are prescribed in the top and bottom boundaries of the domain for velocity and temperature, respectively. At the outlet, a pressure-based condition is used for momentum equation, whereas for energy equation a Neumann condition is assumed. At the cylinder surface, no-slip condition is prescribed for velocity. The Nusselt number ($Nu=hD/\lambda$), which describes the heat transfer characteristics for the flow around the circumference of the cylinder in cross flow is calculated. The predicted local Nusselt number around the circular cylinder in cross flow are in qualitative agreement with experimental measurements [15] and follows the same trends as shown in Figure 1. By comparing the present computation results with the available experimental measurements [15], a fair agreement can be observed for heat transfer characteristics. Although there are some differences between numerical and experimental results, both curves follow the same trend. These differences might be attributed to the large scattering observed in the experiments in the rear zone of the cylinder where heat transfer fluctuations is more random in nature and more complicated to measure [15].

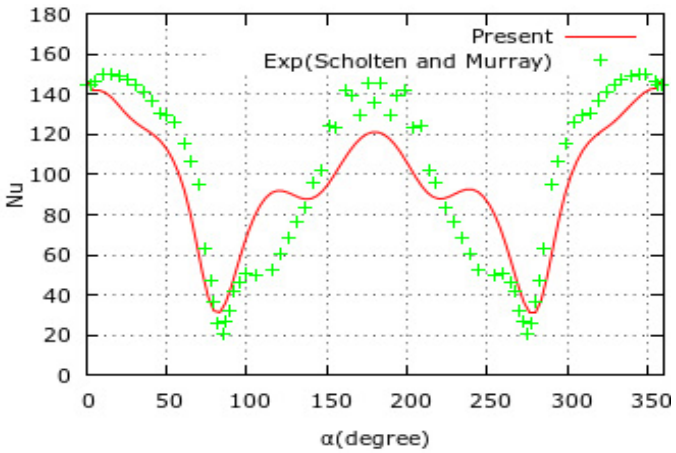

Fig. 1. Variation of the Nusselt number around a cross flow horizontal cylinder and comparison with cross-flow horizontal cylinder and experimental data [15] at Re_D = 21580.

The Nusselt number is maximum at the leading edge or the front stagnation point (fsp) and, decreases smoothly by moving towards the top (or the bottom) of the cylinder. The minimum value occurs at about 85º from the stagnation point of the cylinder, which is associated with flow separation and the formation of a recirculation zone in the near wake. That is, the local separation restricts heat transfer away from the surface and causes the decrease of the Nusselt number. It increases again by approaching to the wake region as the turbulent wake allows heat to be removed.

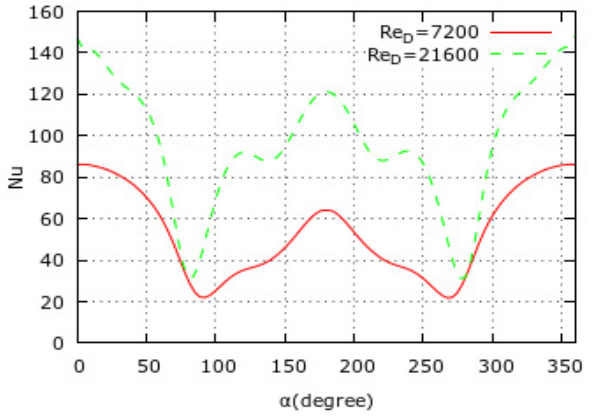

Fig. 2. Comparison of Nusselt number around a circular cylinder in cross flow for two Reynolds numbers: Re_D=7200 and Re_D=21600

Compared to the case of Re_D=7200 (see figure 2), it can be observed the increasing of inertial effect due to the increasing of Reynolds number which lead to earlier separation of the boundary layer. This is clear in the displacement of the minimum Nusselt number at Re_D=21600 towards the stagnation point. The variation of the Nusselt number in the rear zone of the cylinder is smother at Re_D=7200 and new peak is clearly observed for Re_D=21600 (at about α=118º). By increasing the Reynolds number the averaged Nusselt number around the cylinder increases and the difference between the numerical results and experimental measurements becomes more important.

3.2. Wind speed effects on the fluid flow and heat transfer around a PTC

Simulations are conducted to study the wind effect around the PTC for a Reynolds number based on the aperture: $Re_{W1}=3.6\times10^5$ and $Re_{W2}=1\times10^6$. These Reynolds numbers corresponds to realistic working conditions for solar plants, i.e. it corresponds to a wind speed of about 1m/s and 3m/s. Different pitch angles are simulated such as : θ=0º, θ=45º, θ=90º, θ=135º, θ=180º, θ=270º.

The computational domain is defined by 5W in the upstream direction, 20W in the downstream direction, 9 W in the cross direction and πW in the span-wise direction. A constant wind speed is considered in the inlet boundary condition. Slip conditions are fixed in the top and bottom boundaries, while at the outlet a pressure-based condition is used. At the mirror and HCE surfaces, no-slip conditions are prescribed. As for the span-wise direction, periodic boundary conditions are imposed. In a similar manner to the circular cylinder (see section 3.1) a three dimensional extruded mesh is generated. The mesh is refined around the mirror, the HCE and the near wake and then, stretched going away from the collector.

The Prandtl number is set to (Pr=0.7) as for air. The temperatures of the glass cover and ambient air are fixed to T_g=350 K and T_{amb}=300 K, respectively. A Neumann boundary condition is prescribed in the top, bottom and outlet boundaries for temperature. Simulations have been advanced in time until statistical stationary flow conditions have been achieved and the initial transient has been completely washed out. The, average statistics are computed for a sufficient long time which ensures temporal convergence.

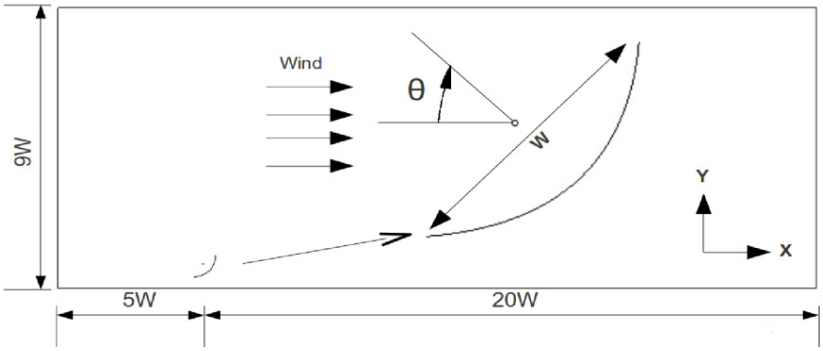

Fig. 3. Computational domain of a parabolic trough solar collector under wind conditions

3.2.1. Averaged forces

The average forces in the parabola have been validated respect to the experimental data [5]. For this purpose, the wind flow is studied around a typical LS-2 parabolic trough collector (without solar receiver) as proposed in the experimental study [5]. Simulations are performed for a full-scale case with a Reynolds number about 2×10^6. After testing several mesh refinement, the predicted aerodynamic coefficients at various pitch angles are shown for finer meshes which are about 7 MCVs with 96 planes in the homogeneous direction. A good agreement can be observed in the comparison with wind-tunnel data [5] and the numerical predictions obtained are within the error-bars of experimental measurements (see figure 4). Discrepancies are most likely due to the flow behavior and ground effects as well as to the scaling up of the Reynolds number used in the measurement model.

Furthermore, calculations are conducted to simulate the fluid flow around an Eurotrough solar collector [16]. The mesh is suited for each case of pitch angle and around the HCE. The construction of the mesh is quite dense and complicated due to the large difference between dimensions of the parabola and the receiver tube. Extensive grid refinement tests are performed and finer meshes are about 12 MCVs. For each angle, the averaged aerodynamic coefficients (drag and lift) are calculated for both Reynolds numbers (Re_{W1} and Re_{W2}) and compared with experimental measurements in figure 4.

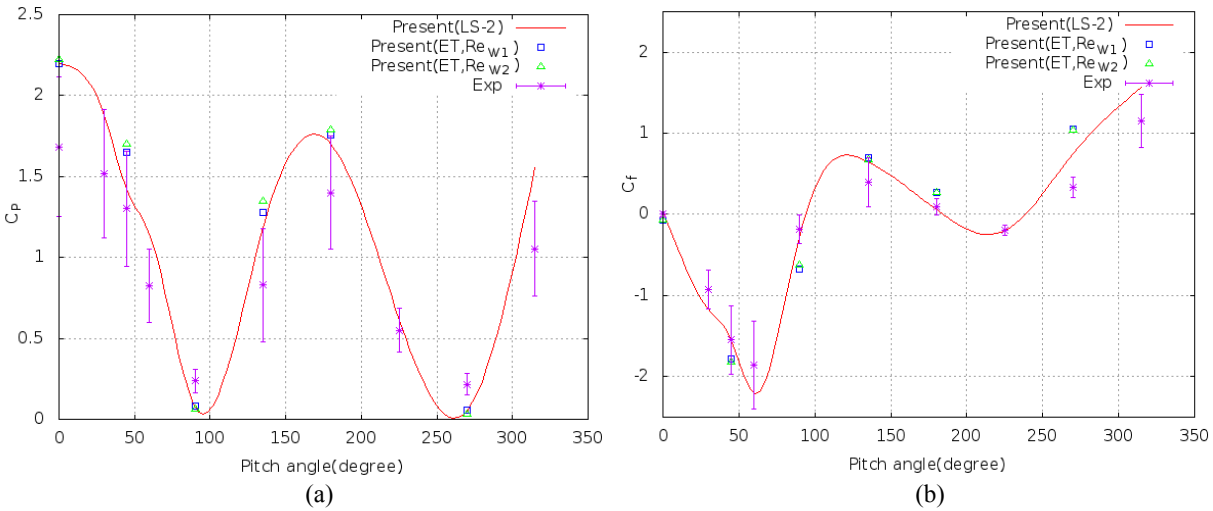

Fig. 4. Predicted aerodynamic parameters for LS-2 and Eurotrough PTC. Wind speed effect and comparison with wind-tunnel data [5]. (a) drag and (b) lift coefficients.

As can be shown from figure 4, the averaged aerodynamic coefficients for Eurotrough PTC at $Re_{W2}=1\times10^6$ exhibit an almost identical profile to those observed at $Re_{W1}=3.9\times10^5$ which proves the stability of aerodynamic coefficients at these range of Reynolds numbers. However, the predicted drag and lift coefficients are strongly influenced by the pitch angle. There are also some differences between numerical results of LS-2 PTC and Eurotrough PTC which are due mainly to the geometry adopted and the complexity of the mesh used in Eurotrough simulations to take into account the presence of the HCE. This involves a small time step (about 5×10^{-6}) and long time of calculation to reach the statistical average. The zero pitch angle presents the maximum horizontal drag force (C_P) and it decreases by moving the parabolic trough toward the horizontal position. However, the lift coefficient (C_f) increases by approaching to the stow mode where the concave surface of the trough is facing the ground. The maximum absolute lift coefficient occurred at about 60º. It is worth noting that the independence of averaged aerodynamic coefficients with Reynolds numbers is also commented in other numerical and experimental results [5,17,18] however it was mentioned that it could be affected where the leading edge is close the alignment with the stream causing some errors on the lift coefficient [17] .

3.2.2. Instantaneous flow structures

Instantaneous flow structures are studied for different pitch angles and wind speeds. The variation of drag and lift coefficients observed in the previous section can be better understood by analyzing the instantaneous flow around the PTC. The streak of flow stream known as shear layer is observed in the vicinity of the parabola. The shear layer separation and its trajectory depend on the pitch angle. For instance, instantaneous velocity field for different pitch angles (θ=0º, θ=45º and θ=90º) and both Reynolds numbers are depicted.

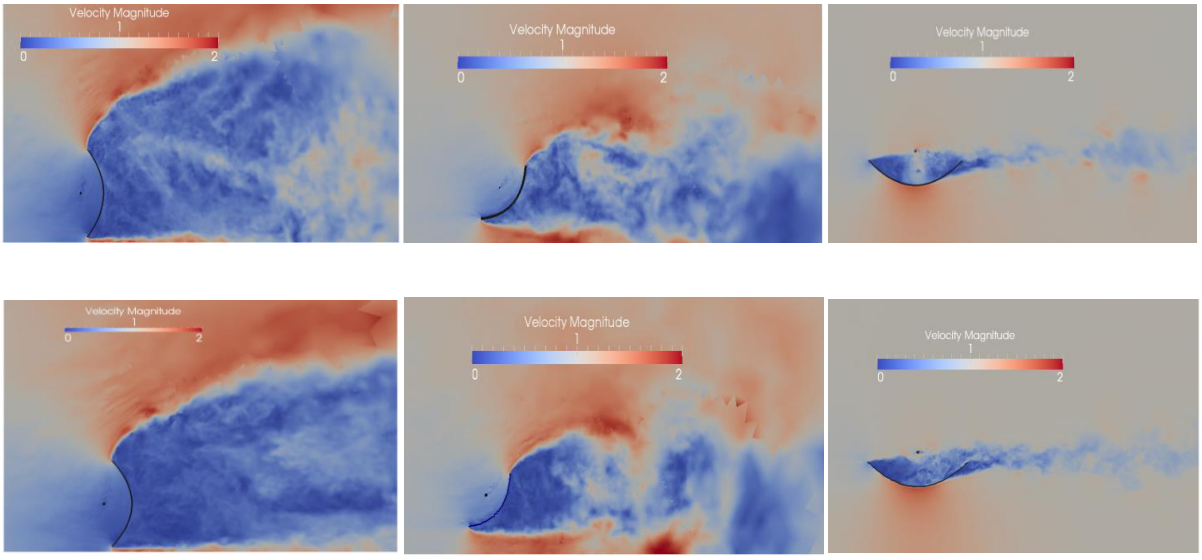

(a) (b) (c)

Fig. 5. Instantaneous velocity field around the PTC for different pitch angles: (a) θ=0º, (b) θ=45º and (c) θ=90º and Reynolds number: Re_{W1} (first row) and Re_{W2} (second row).

For both wind speeds, a large separated zone that follow the curvature of the parabola is observed at θ=0º. The turbulent flow in the detached region produces a large depression region in the back of the PTC being the responsible for the large value of drag coefficient obtained. By increasing the Reynolds number, the shear layer is

reduced and becomes more compact. With the increase of the pitch angle from θ=0º to θ=90º the separated zone is continuously reduced which provokes the reduction of drag forces in the PTC surface.

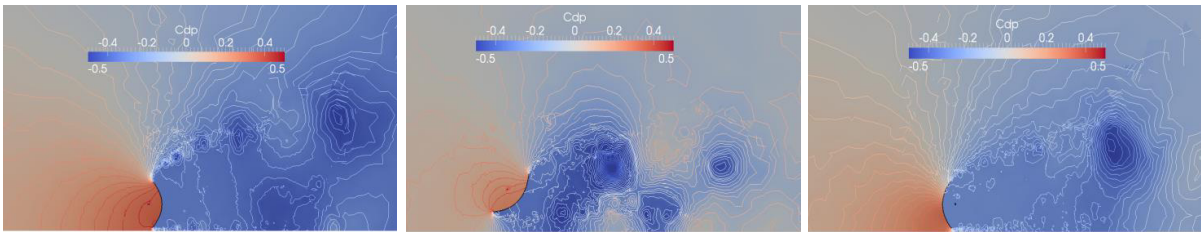

Fig. 6. Instantaneous pressure contours for pitch angle: (a) θ=0º, (b) θ=45º and (c) θ=180º at Re_2

According to the instantaneous pressure map (figure 6), the flow at pitch angle 0º, 45º and 180º separates laminarly from the parabola surface near to the leading edge. Vortex breakdown occurs at the end of the laminar shear layer as a consequence of the instabilities developed by the action of Kelvin-Helmholtz mechanism. These instabilities are presented by small-scale vortices which form within the separated shear layer. The frequency at which these instabilities develop is much higher than that of the vortex shedding mechanism. As the distance from the leading edge increases, these instabilities increase in amplitude until transition to turbulence occurs. This is similar to the phenomena observed in shear layers developed in other bluff bodies [19]. By moving the flow downstream, the small-scale vortices in the shear layer increase and accumulate into larger structures with low pressure at their core similar to the von Kármán-like vortex street.

3.2.3. Time averaged flow

After all transient are washed out, statistics are collected over 30 time units (tU/W). Time-averaged flow is studied for different pitch angles and compared for both Reynolds numbers. Different structures and recirculation regions are encountered around the collector and the HCE. These flow structures are strongly related to the collector orientation and the pitch angle. Several recirculation regions are formed around the HCE depending on the pitch angle and the position of the PTC.

The effect of the wind speed on the structures and recirculation regions observed around the PTC has been also assessed. By increasing the Reynolds number, the flow pattern does not change and the recirculation regions are similar to those found at the lower Reynolds number with small variation of the recirculation length behind the parabola and the solar receiver as shown in figure 7 and 8.

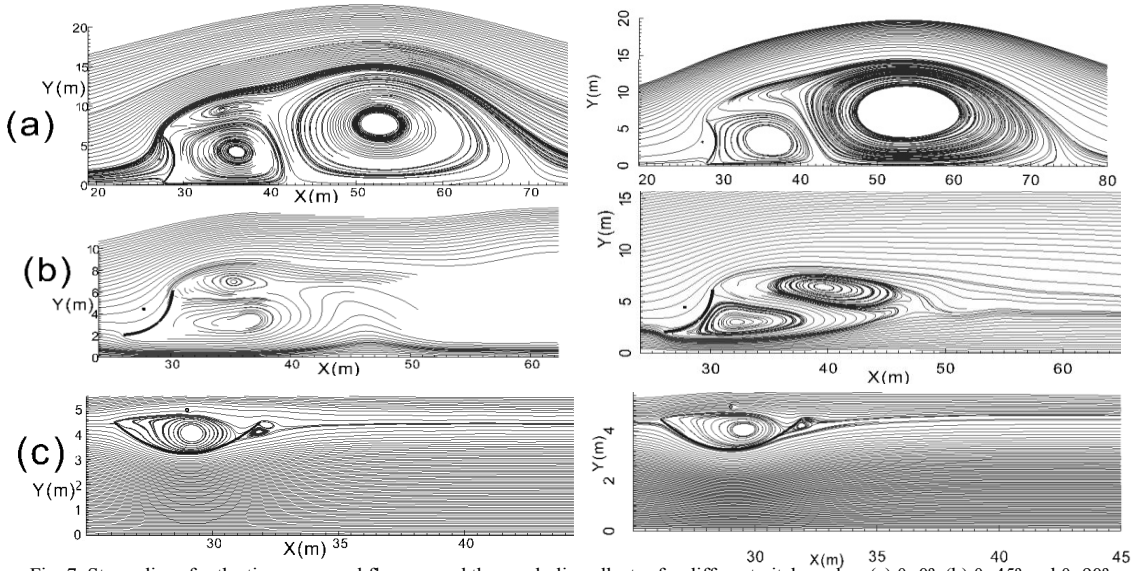

Fig. 7. Streamlines for the time-averaged flow around the parabolic collector for different pitch angles: (a) θ=0º, (b) θ=45º and θ=90º. Comparison between both Reynolds numbers: Re_{W1} (left) Re_{W2} (right).

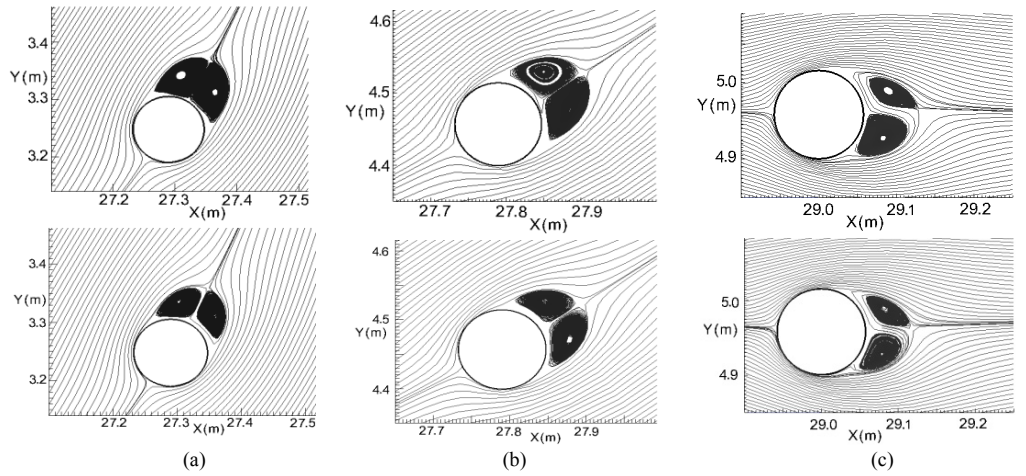

Fig. 8. Streamlines for the time-averaged flow around the HCE for different pitch angles: (a) θ=0º, (b) θ=45º and θ=90º. Comparison between both Reynolds numbers: Re_{W1} (first row) Re_{W2} (second row).

The recirculation length for different pitch angles and for both Reynolds number is determined and presented in table1. It can be seen from this table that the recirculation length is almost in the same range for both Reynolds numbers. This similarity has been also depicted in the comparison of averaged streamlines for both Reynolds numbers (see figure 7). However, it is observed that the recirculation length increases with the Reynolds number when the concave surface of the parabola is exposed to the wind direction, i.e θ<90º and decreases for the convex surface configuration (θ>90º).

Table 1. Variation of the ratio of the non-dimensional recirculation length to collector aperture with pitch angle and comparison between both Reynolds numbers.

	θ=0º	θ=45º	θ=90º	θ=135º	θ=180º	θ=270º
$Re_{W1}=3.9\times10^5$	7.56	2.21	0.09	1.6	9	0.2
$Re_{W2}=1\times10^6$	8.32	3.06	0.1	1.47	8.3	0.17

3.2.4. Heat transfer around HCE

Numerical simulations are carried out to study the heat transfer around the HCE and determine the effect of the pitch angle and the wind speed on the heat transfer from the solar receiver. As it has been discussed in the previous work [10], the convection occurred around the HCE is divided into forced convection (for pitch angles of θ=0º, 45º, 90º and 270º) and mixed (free and forced) convection (for pitch angles of 135º and 180º). In figure 9, the distribution of the local Nusselt number for different pitch angles together with the comparison between different Reynolds numbers and the cross flow case are shown. According to this figure, the profile of Nusselt number around the HCE is affected with the pitch angle and the displacement of the fluid structure around the HCE due to the tilt of the parabola. At higher wind speed, the profile of Nusselt number follows a similar trend to the profile of Nusselt number for the lower speed Re_1 with a higher magnitude. It was also observed that the peaks are more significant and larger for higher wind speed. The effect of the parabola and the ground becomes more significant with increasing the Reynolds number. This can be clearly observed in the horizontal positions (working and stow modes), i.e. θ=90º and θ=270º, where the distribution of the Nusselt number is no longer similar to the circular cylinder in cross flow as it was valid for lower wind speed especially in the rear zone (see figure 10). At these positions, the combined effect of the parabola and the ground tend to reduce the large fluctuations encountered in the near wake. This phenomenon leads to a smoother distribution of the Nusselt number in the rear zone and a similar trend compared to the low wind speed case. Table 2 summarizes the averaged Nusselt number around the HCE for both Reynolds numbers and various pitch angles. In all the pitch angles, the averaged Nusselt number increases with the Reynolds number. It is maximum when the parabola is placed at the working position (θ=90º) and it is minimum when the HCE is placed behind the PTC (θ=180º). Although it is higher at the horizontal positions, the magnitude of the Nusselt number in the stow position (θ=270º) is more affected by the ground and the averaged Nusselt number is much lower than the working position compared to the lower wind speed case.

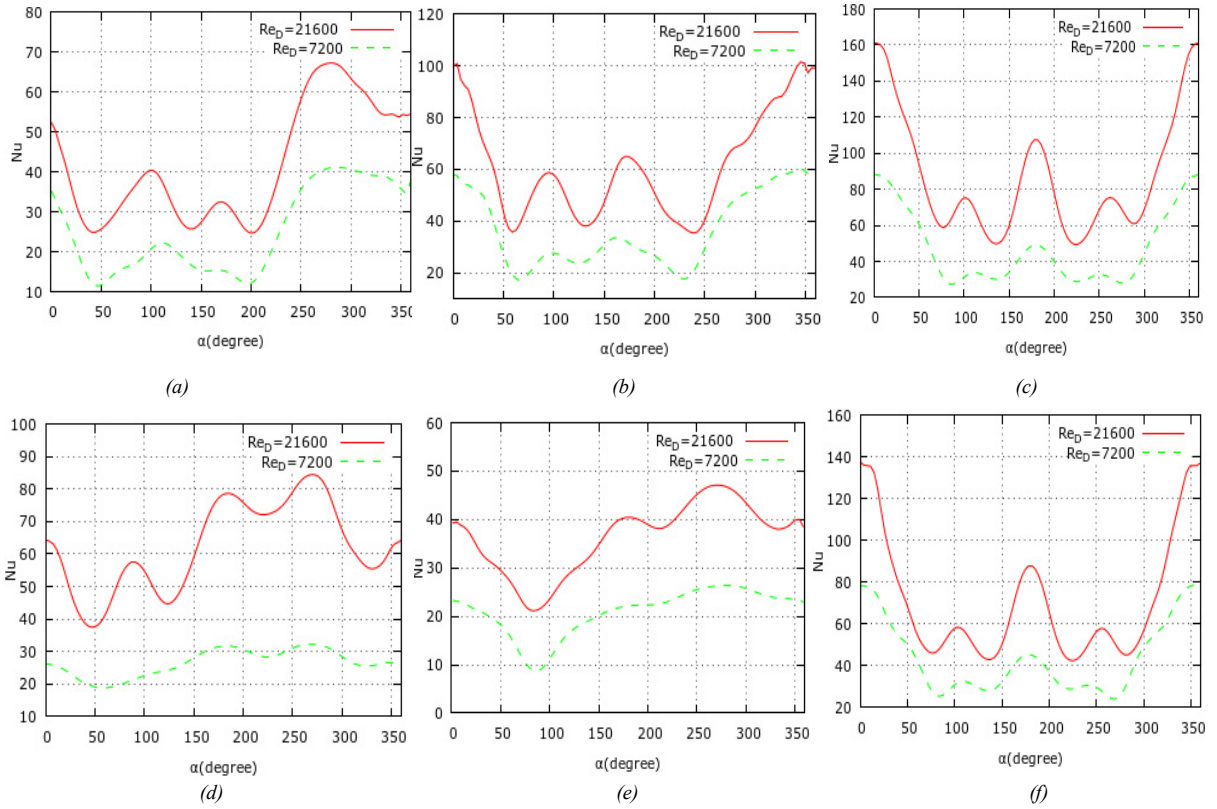

Fig. 9. Variation of the local Nusselt number around the HCE for different wind speed at (a) θ =0º , (b) θ =45º, (c) θ =90º, (d) θ =135º, (e) θ=180º, (f) θ =270º

For different cases of pitch angles, the magnitude of the average Nusselt number is reduced compared to the cross-flow condition. This reduction is desirable since it reduces heat losses from the HCE and improves the thermal efficiency.

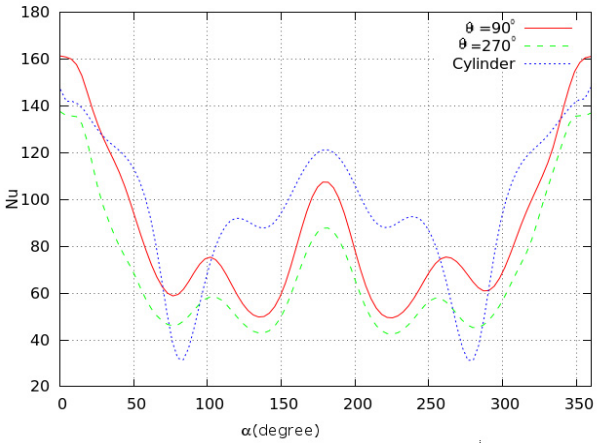

Fig. 10. Comparison of the profile of Nusselt number for horizontal positions (θ=90º and θ=270º) with the Nusselt number for the circular cylinder in cross flow case (without parabola) at Re_D=21600.

Table 2. Variation of the averaged Nusselt number with pitch angle and comparison between both Reynolds numbers.

	θ=0º	θ=45º	θ=90º	θ=135º	θ=180º	θ=270º
$Re_{W1}=3.9\times10^5$	24.5	36.4	47.4	25.1	22.5	43.4
$Re_{W2}=1\times10^6$	41.6	61	87.8	54.6	36.31	70.3

4. Conclusions

In the current work, a numerical study based on LES models for the simulation of the fluid flow and heat transfer around a parabolic trough solar collector and its receiver tube is performed. The effects of wind speed and pitch angle on the aerodynamic behavior and heat transfer characteristics around a PTC have been addressed. First, the effect of the wind speed on the heat transfer coefficient around a circular cylinder in a cross flow has been assessed. Then, a wind analysis is carried out around a typical Eurotrough solar collector to calculate the aerodynamic coefficients and the heat exchange between the HCE and the air ambient. Instantaneous velocity and pressure maps have been compared for different pitch angles and wind speeds and small-scale shear layer stabilities have been observed near to the edges of the parabola. Different structures and recirculation regions have been identified in the time-averaged flow around the PTC and the HCE. These structures are quite similar for both studied Reynolds numbers. However the recirculation length increases when the parabola is oriented to the wind direction (θ<90º) and decreases in the opposite case. Heat transfer coefficients around the HCE are also calculated and compared for different pitch angles and wind speeds. The distribution of Nusselt number for the higher wind speed shows a similar trend to the lower wind speed with higher magnitude and significant peaks.
Even though, the study presented in this work is useful for analyzing the fluid flow and heat transfer around an isolated PTC at different working conditions (wind speeds, pitch angles, etc); actual PTCs are located within solar field. Thus, the wake behind these collectors may affect the inlet working conditions of the PTCs located downstream. Therefore, the study of an array of PTC needs to be addressed in future studies.

Acknowledgements

This work has been partially financially supported by the "Ministerio de Economía y Competitividad, Secretaría de Estado de Investigación, Desarrollo e Innovación" Spain (ref. ENE2010-17801), by the "Agencia Española de Cooperación Internacional para el Desarrollo" (AECID) and by the collaboration Project between Universitat Politècnica de Catalunya-BarcelonaTech and Termo Fluids S.L.

References

[1] Forristall R. Heat transfer analysis and modeling of a parabolic trough solar receiver implmented in engineering equations solver. Tech rep. National Renewable Energy Laboratory (NREL); 2003.
[2] García-Valladares O, Velázquez N. Numerical simulation of parabolic trough solar collector: improvement using counter flow concentric circular heat exchangers. Int J Heat Mass Transfer 2009; 52(3-4):597-609.
[3] Padilla R, Demirkaya G, G Goswami Y, Stefanakos E, Rahman M. Heat transfer analysis of parabolic trough solar receiver. Applied eneenergy 2011;88:5097-110.
[4] Hachicha AA, Rodríguez I, Capdevila R, Oliva A . Heat transfer analysis and numerical simulation of a parabolic trough solar collector. Applied Energy (2013), 111: 581–592.
[5] Hosoya N, Peterka JA, Gee RC, Kearney D. Wind tunnel tests of parabolic trough solar collectors, March 2001-August 2003, NREL/SR Report 550-32282 (2008).
[6] Gong B, Wang Z, Li Z, Zhang J, & Fu X. Field measurements of boundary layer wind characteristics and wind loads of a parabolic trough solar collector. Solar Energy 2012;86:1880-98.
[7] Naeeni N, Yaghoubi M. Analysis of wind flow around a parabolic collector (1) fluid flow Renewable Energy 2007; 32 :1898–1916.
[8] Naeeni N, Yaghoubi M. Analysis of wind flow around a parabolic collector (2) fluid flow Renewable Energy 2007; 32: 1259-1272.
[9] Rodi W. Comparison of LES and RANS calculations of the flow around bluff bodies. J Wind Eng Indus Aerodynam 1997;69–71:55–75.

[10] Hachicha AA, Rodríguez I, Castro J, Oliva A. Numerical simulation of wind flow around a parabolic trough solar collector. Applied energy 2013, 107; 426-437.
[11] Rodríguez I, Borrell R, Lehmkuhl O, Pérez-Segarra C, Oliva A. Direct numerical simulation of the flow over a spher at Re = 3700. J Fluid Mech 2011(279):263–87.
[12] Lehmkuhl O, Baez A, Rodríguez I, Pérez-Segara C. Direct numerical simulation and large-eddy simultaions of the turbulent flow around a Naca-0012 airfoil.In: ICCHMT 7; 2011.
[13] Rodríguez I, Lehmkuhl O, Borrell R, Oliva A. Flow dynamics in the wake of a sphere at sub-critical Reynolds numbers. Comput Fluids 80 (2103); 233-243.
[14] Lehmkuhl O, Pérez-Segarra CD, Borrell R, Soria M, Oliva A. TERMOFLUIDS: a new parallel unstructured CFD code for the simulation of turbulent industrial problems on low cost PC cluster. Proceedings of the 2005 parallel computational fluid dynamics conference, vol. 67. Springer; 2007. p. 275–82.
[15] Scholten J, Murray D. Unsteady heat transfer and velocity of a cylinder in cross-flow – I. Low freestream turbulence. Int J Heat Mass Transfer 1998;41(10):1139–48.
[16] Lüpfert E, Geyer M, Schiel W, Esteban A, Osuna R, Zarza E, et al. EUROTROUGH design issues and prototype testing at PSA. In: Proceedings of ASME international solar energy conference-forum 2001: 289–394.
[17] Randall D E., McBride D. D, Tate R. E. Parabolic trough solar collector wind loading. In American Society of Mechanical Engineers, Energy Technology Conference and Exhibition 1980; 1: 18-20.
[18] Christo, F. C. Numerical modelling of wind and dust patterns around a full-scale paraboloidal solar dish. Renewable Energy 2012; 39:356-366.
[19] Prasad, A., Williamson, C., 1997. The instability of the shear layer separating from a bluff body. Journal of Fluid Mechanics, 375–492.